Background Noise Mitigation in Deep-Space Optical Communications Using Adaptive Optics

S. Lee,[1] K. E. Wilson,[1] and M. Troy[2]

Over the last decade, adaptive optics technology has moved from the purview of a Department of Defense laboratory to astronomical telescopes around the world, and recently to industry, where adaptive optics systems have been developed to correct atmospheric-induced signal fades on high-bandwidth horizontal-path optical links. As JPL develops optical communications technology for high-bandwidth optical links from its deep-space probes, we are exploring the application of adaptive optics to the optical deep-space receiver to improve the quality of the link under turbulent atmospheric and high-background conditions. To provide maximum communications support, the operational deep-space optical communications receiver will need to point close to the Sun or to a bright Sun-illuminated planet. Under these conditions, the background noise from the sky degrades the quality of the optical link, especially when the atmospheric seeing is poor. In this work, we analyze how adaptive optics could be used to mitigate the effects of sky and planetary background noise on the deep-space optical communications receiver's performance in poor seeing conditions. Our results show that, under nominal background sky conditions, gains of 4 dB can be achieved for the uncoded bit-error rate of 0.01.

I. Introduction

Limitations of size, mass, and power on the spacecraft transmitter make optical communications an attractive technology for supporting future high-bandwidth instruments on deep-space probes. Yet, as in all deep-space missions constrained by available transmitter power, the optical communications systems designer will need to optimize the link performance by maximizing the receiver gain by enlarging the collection aperture. Although larger telescopes allow for detection of weak light levels at optical frequencies, atmospheric turbulence typically limits the resolution to that of a 10-cm telescope. Degraded telescope resolution will require the receiver field of view (FOV) to be expanded to maximize the downlink signal collected. For daytime links, expanding the FOV will decrease the signal-to-noise ratio (SNR) at the receiver due to the increase in background flux.

---

[1] Communications Architectures and Research Section.

[2] Interferometry and Advanced Optical Systems Section.

The research described in this publication was carried out by the Jet Propulsion Laboratory, California Institute of Technology, under a contract with the National Aeronautics and Space Administration.

Three of the strategies for mitigating the effect of background light on the optical link are (1) spectral filtering, (2) advanced signal modulation, and (3) spatial filtering. Spectral filtering uses narrowband filters to increase SNR. However, very narrow optical filters add a higher degree of complexity to the receiver by requiring the filter to track the Doppler shifts due to the relative velocities between the spacecraft and Earth. Pulse-position modulation (PPM) is the format of choice for deep-space communications. In this modulation format, a word is determined by the location of the laser pulse in a predefined series of M time slots, with the throughput rate inversely proportional to the slot width. The narrower the pulse width, the less the background noise. Yet, generating high-power clock-synchronized sub-nanosecond laser pulses is challenging. The final strategy, spatial filtering, can suppress the background noise. However, this requires the implementation of the adaptive optics (AO) techniques used by astronomers to reduce the effects of atmospheric turbulence. Conceptually, the adaptive detector arrays can achieve a certain degree of spatial filtering (up to 5 dB for the high-background case) with variable weighting on the detector elements, which is proportional to the signal intensity [1].

Adaptive optics allows correction of atmosphere-induced wavefront aberrations and enables efficient spatial filtering of the received signal and near diffraction-limited performance of the receiver. In this article, we describe the effects of atmosphere-induced aberrations (atmospheric "seeing") and optical background noise on the optical link. We analyze the link with and without adaptive optics, and our results show that, depending on "seeing" and the background noise level, in excess of a 5-dB gain can be realized by using adaptive optics in a photon-counting channel.

An earlier study [2] first reported similar results for a particular seeing condition (nominal seeing of 15 μrad, corresponding to an r_0 of 7 cm) with background limited to the daytime. The reported AO gains (signal reduction at a bit-error rate (BER) of 0.01 for PPM orders of 16, 64, and 256) for three background levels (3-km altitude daytime clear sky, daytime nominal sea level, and sunlight scattering from optics) were 1 to 6 dB as compared with the non-AO case. This article expands the first study to more general and realistic cases. In particular, we incorporated (1) the seeing statistics representing the range of real operating conditions measured at the Table Mountain Facility (TMF) at Wrightwood, California, which houses a 1-m telescope dedicated to optical communications, instead of single-point seeing conditions, (2) daytime background fluxes estimated using parameters (e.g., Sun–Earth–probe (SEP) angle, observation angle, altitude) used in actual mission operations, and (3) both daytime and nighttime background estimates, where the nighttime background flux from the Sun-illuminated planets was shown to have large background flux, sometimes exceeding the sky background. To estimate the gain using AO, we followed the approach of the earlier study, i.e., estimating the signal reduction at a BER of 0.01 for a certain PPM order. For the PPM order, we chose $M = 64$. The gain differences with other PPM orders were shown in [2].

In Section II, we discuss atmospheric seeing and its relationship to the communications detector field of view. In Section III, we present the noise sources, i.e., the daytime sky and the Sun-illuminated planets, and determine the background noise level as seen from the 1-m Optical Communications Telescope Laboratory (OCTL) telescope, and we extend this analysis to a 5-m aperture. We compare the background noise at the receiver with and without adaptive optics in Section IV, and from the BER plots, we calculate the performance gain afforded by adaptive optics under a variety of atmospheric conditions. We summarize our results in Section V.

II. Atmospheric Seeing and the Communications Detector FOV

Atmospheric seeing is defined as the blurring of the image of a point source by atmospheric turbulence. It is measured as the full width at half the maximum (FWHM) of the signal integrated over a period of several seconds, and it varies with wind speed, temperature, and altitude. Figure 1 shows recent seeing data from the OCTL at the Table Mountain Facility, taken through an 810-nm interference filter. The data cover the months March, April, and June of 2004 and represent both daytime and nighttime

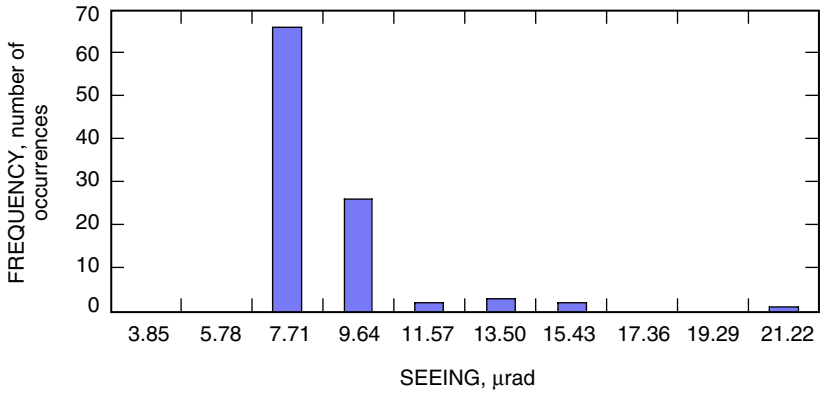

Fig. 1. Histogram of atmospheric seeing at the OCTL for the months of March, April, and June 2004. Measurements were made using the star Polaris and include both daytime and nighttime measurements. The data are corrected for zenith angle and a wavelength of 1064 nm.

measurements.[3] The measurements were made of the star Polaris, fixed at approximately a 55-deg zenith angle as seen from the OCTL. The 810-nm filter used to provide contrast of the star image against the sky background in the day also was used for nighttime seeing measurements. The expression for seeing was corrected to the 500-nm wavelength. The seeing data have been corrected to 500 nm using Eq. (1) [3, p. 45] and compensated for the air mass at a 55-deg zenith angle, ξ, using the relationship in Eq. (2) [3, p. 103]:

$$\theta_1 = \theta_2 \left(\frac{\lambda_2}{\lambda_1} \right)^{1/5} \tag{1}$$

$$\theta(\xi) = \theta_0 \sec^{3/5}(\xi) \tag{2}$$

The results show that the seeing ranges from 4 μrad to 22 μrad at the zenith angle. At the extreme of operating points, an elevation angle of 20 deg, the seeing can be more than 40 μrad. For the middle point of the operating range (between an elevation angle of 20 deg and the zenith angle), the seeing ranges between 5 and 25 μrad, which will be used in Section IV as the seeing range to compare the signal gains for a fixed BER with and without AO.

The size of the corresponding seeing disk at the 1064-nm communications wavelength can be calculated from Eq. (1). The calculations show that the seeing disk at 1064 nm is approximately 14 percent smaller than that at 500 nm. For the communications link, we specify a receiver FOV corresponding to a 1-dB loss or 80 percent energy enclosed disk. The relationship between the seeing disk and the 80 percent energy enclosed disk is given in Eq. (3) and plotted in Fig. 2; it is derived in Appendix A:

$$\mathrm{FOV}_{80\%} = 1.5238\,\mathrm{FWHM} \tag{3}$$

[3] D. Mayes, "TMF Seeing Statistics," JPL Interoffice Memorandum (internal document), Jet Propulsion Laboratory, Pasadena, California, 2004.

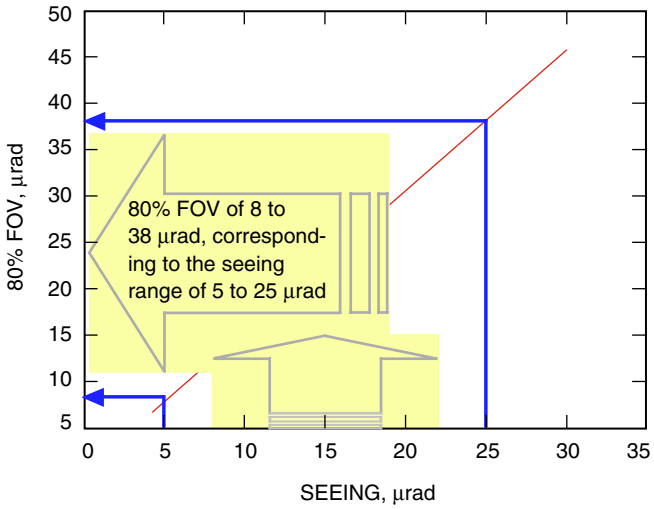

Fig. 2. Seeing versus FOV for 80% energy for a 1064-nm downlink beam. To receive 80% energy on the communication detector, the FOV needs to be at least 53% larger than the seeing disk.

III. Background Noise Sources and Their Effects

Sky radiance is the dominant noise source during the daytime, and the Sun-illuminated planet is during the nighttime. The noise levels vary with mission parameters such as the phase angle, the planet, the wavelength, and the range. We analyze the background light levels at the 1064-nm deep-space communications wavelength for the sky radiance at a 3-deg Sun angle, the worst-case condition for the Mars Lasercomm Demonstration project, and for the four planets Venus, Mars, Jupiter, and Saturn.

Sky background levels depend both on the Sun's elevation angle and on the look angle with respect to the horizon. We have limited our analysis to 20-deg elevation, our current operational constraint.

Figure 3 is a MODTRAN calculation of the sky radiance from the visible to the near-infrared. Sky radiance is due to Rayleigh scattering of sunlight by the atmosphere, and the figure shows the characteristic $1/\lambda^4$ decrease in Rayleigh scattering with increasing wavelength and the effect of water-vapor absorption bands on the sky radiance around 0.95 μm and 1.1 μm.

Figure 4 is a plot of the background photons as a function of the receiver field of view for a 1-m and a 5-m aperture, corresponding to the OCTL and Palomar telescopes, respectively. This is assumed to be through a 1-Å filter. From Fig. 1, a 50-μrad FOV corresponds to the worst daytime seeing expected at the OCTL at a 20-deg elevation.

The background noise from the planet will depend on the angular size of the planet relative to the detector FOV and the planet's geometric albedo. Table 1 gives the apparent angular size of the four planets considered at opposition and at conjunction.

The background photons from these planets through the two telescope apertures under consideration are plotted in Figs. 5(a) and 5(b) as a function of FOV. The filter width again is 1 Å. For resolved images of the planet, the albedo will vary with planetary surface features and wavelength. This higher-order effect is not considered in our analysis. The figures show that Venus has the highest background noise. This is because of its size and proximity to Earth. A comparison of Figs. 4 and 5(a) shows that the photon flux from the planet Venus exceeds that of the day sky. The background noise from Mars is limited by the planet's irradiance at conjunction (daytime) and by atmospheric seeing (20 μrad) at

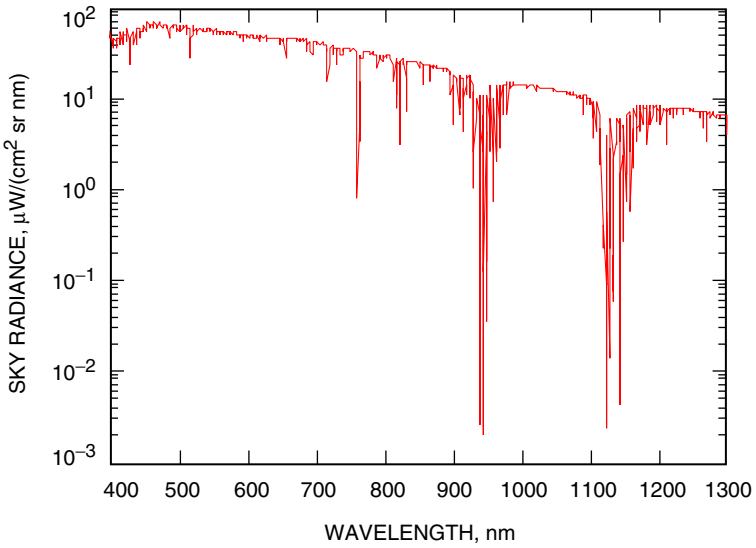

Fig. 3. Sky radiance at a 3-deg SEP angle, assuming a 20-deg elevation angle, a 70 ± 3 deg Sun zenith angle, clear sky, and a 2.2-km altitude.

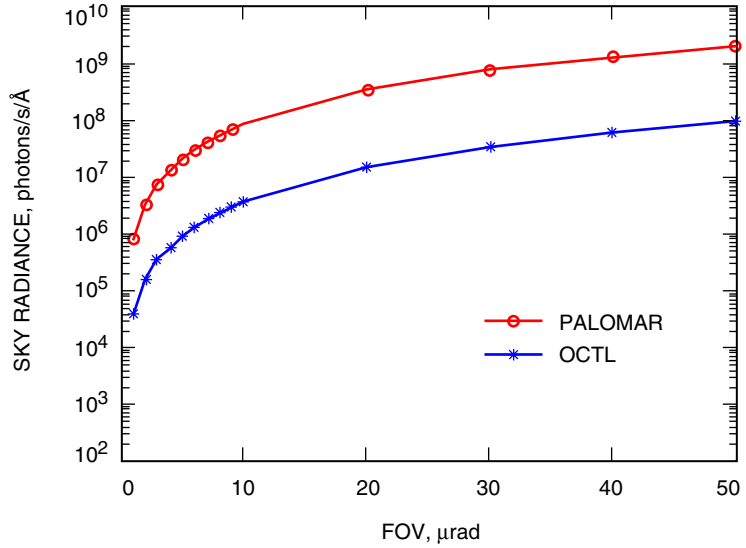

Fig. 4. Sky background estimates at the Palomar and OCTL telescopes as a function of FOV for an SEP angle of 3 deg.

Table 1. Apparent angular sizes of planets.

Planet	Conjunction, μrad	Opposition, μrad
Venus	49	310
Mars	19	120
Jupiter	150	230
Saturn	73	100

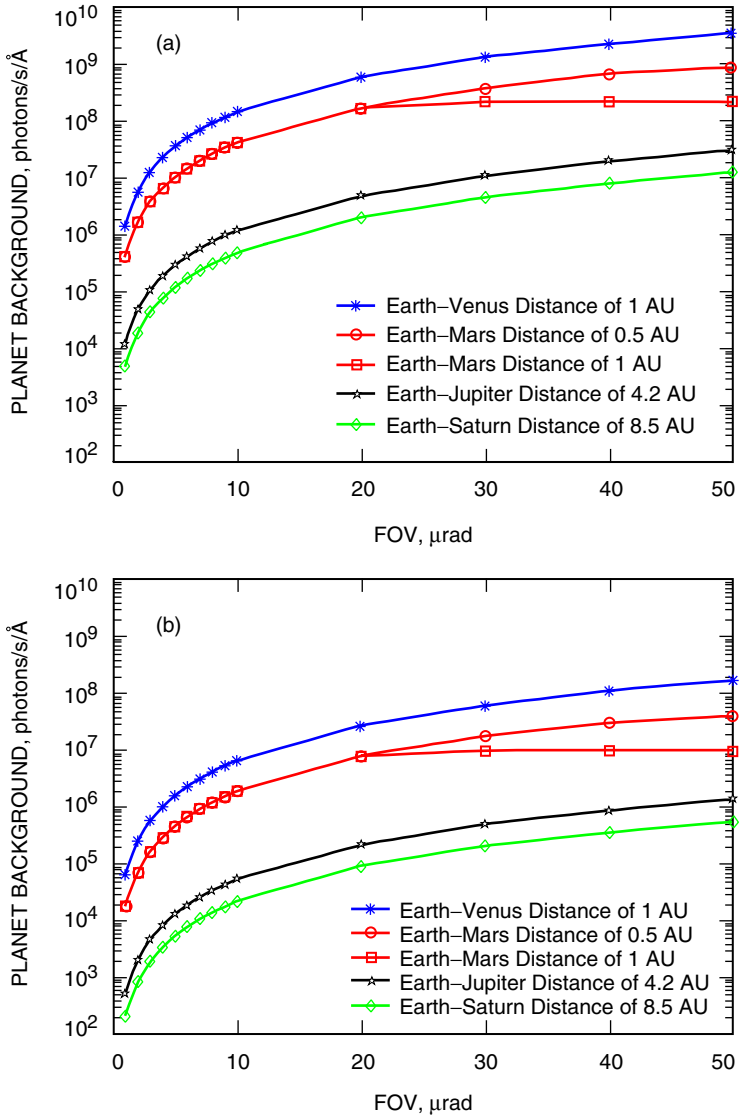

Fig. 5. Background photons from planets (photons/s) as a function of FOVs (a) at nighttime for the Palomar telescope and (b) for the OCTL telescope.

opposition (nighttime). This is shown in Figs. 5(a) and 5(b), where for the 1-AU range the number of background photons is constant for FOVs greater than 20 μrad.

The apparent sizes of Jupiter and Saturn exceed the nominal seeing-limited FOV of the receiver. In the absence of atmospheric turbulence compensation, the background noise in a communications link with a spacecraft in orbit around either of these planets will be determined by the albedo variation and by the FOV dictated by atmospheric seeing at conjunction or opposition.

Figures 6(a) and 6(b) give the sky background noise per slot (1 ns) as a function of FOV in a 1-Å bandwidth at OCTL and Palomar PPM receivers. The figures show the criticality of reducing the background noise. The background noise rapidly increases as the FOV increases—ranging from less than 0.0001 photon to about 2 photons per slot.

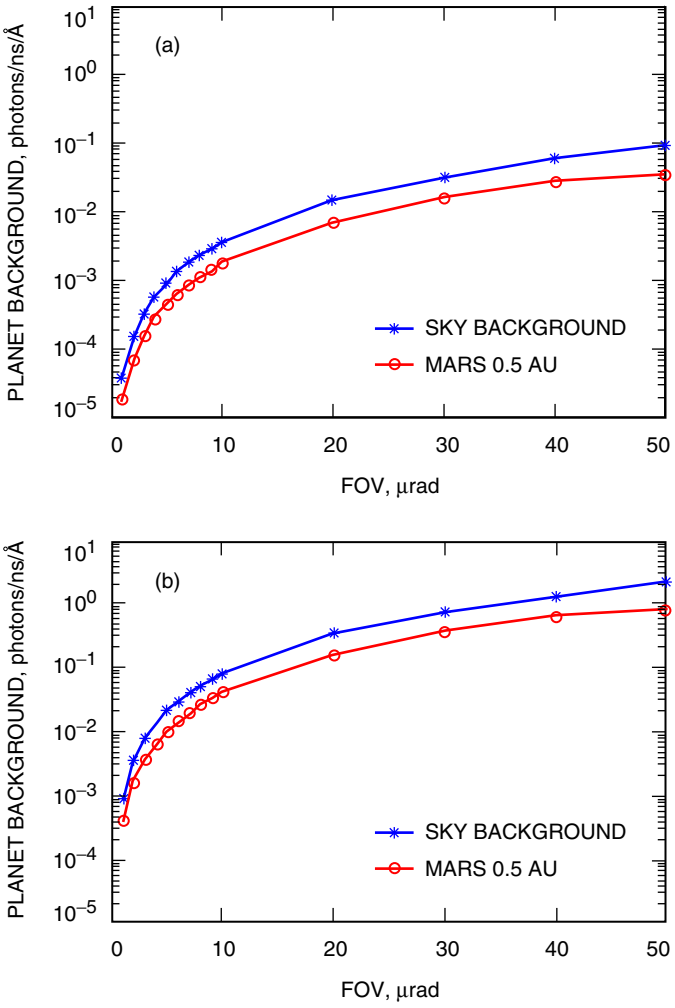

Fig. 6. MODTRAN-calculated sky background photons from the day sky (3-deg SEP) and Mars background photons for 1 ns and a 1-A filter at (a) the OCTL and (b) the Palomar observatory.

Mars and Venus are the planets for which the background noise is highest. Mars background photons range from less than 0.0001 photon to more than 0.9 photons per slot. The background photons from Venus are a factor of 3.5 greater than that of Mars. We focus our subsequent analysis on the Mars-to-Earth link.

IV. Comparison of Optical Communications Link Performance Realized With and Without Adaptive Optics

A. The Communications Link

Table 2 shows three operating points—best, nominal, and worst-case conditions for the first deep-space optical communications link (Mars–Earth), scheduled to launch in 2009.[4] The three cases represent the best case, nominal case, and worst case in terms of data rate. The atmospheric conditions are closely

[4] A. Biswas and B. Moision, "MLCD Operating Points," JPL Interoffice Memorandum 331.2004.07.1 (internal document), Jet Propulsion Laboratory, Pasadena, California, July 1, 2004.

Table 2. Three operating points for a deep-space optical link.

Symbol	Definition	Operating points		
		Best	Nominal	Worst
P	Laser transmit power, W	5	5	5
T_s	Slot width, s	1.6×10^{-9}	3.84×10^{-8}	3.07×10^{-7}
FOV	Field of view, μrad	15.2	17.1	23.1
w	Filter width, nm	0.1	0.1	0.1
λ_b	Incident background photons/s	6.3×10^{6}	4.0×10^{7}	4.5×10^{8}
λ_s	Incident signal photons/s	8.3×10^{7}	1.0×10^{7}	8.13×10^{6}
η	Detector efficiency	0.3	0.3	0.3
M	PPM order	64	64	64
n_b	Noise photons/slot $n_b = \lambda_b \eta T_s$	3.0×10^{-3}	0.5	41.2
R	Code rate	1/2	1/2	1/2
L	Required signal margin, dB	3	3	3
n_s	Estimated required signal photons/pulse $n_s = \lambda_s M \eta 10^{-L/10} T_s$	1.3	3.7	24.0
T	Throughput, mega-bits per second $T = R \log_2(M)/MT_s$	29.3	1.2	0.2

related for the three cases, where the seeing is increasing proportionally among the best, nominal, and worst cases. The corresponding seeing for 1064 nm is 9.5 μrad, 10.7 μrad, and 14.5 μrad for the best, nominal, and worst cases, respectively. The noise and signal-photon levels were estimated from the 2-year mission parameters during the orbit phase. The signal photons were calculated using a 5-W laser coupled to a 30-cm transmit aperture, with a 5-m receive telescope. Notice that the incident background photons in Table 2 and Fig. 4 are equivalent.

Noise photons are primarily sky background at the corresponding SEP and zenith angles. The chosen line filter width was 1 A, which somewhat minimizes the background noise in terms of today's technology in regard to the spectral background noise-reduction approach. However, this can impose some challenges in terms of temperature tuning and alignment calibration.[5] Also notice that the slot width varies due to the laser peak-power limitations, which cannot increase peak power indefinitely for a short pulse width. The background flux scales directly with the filter width, slot width, and detector efficiency.

B. Adaptive Optics and Background Noise Suppression: The Mars Link

The Fried coherence length, r_o, defines the aperture size over which the mean-square wavefront error (WFE) is 1 rad^2. It is, therefore, r_o, and not the aperture size that defines the ability of the telescope to resolve the image of a point source. Therefore, although large receiver apertures provide the requisite gain in the communications link, the FOV of the receiver is determined by the coherence cell size of the atmosphere and not by the aperture diameter, D. The atmospheric seeing, θ, relates to the Fried coherence cell size by $r_o = \lambda/\theta$, where θ is the FWHM of the seeing disk. The Fried coherence cell size at the 1.06-μm wavelength for the most probable seeing is 12.3 cm.[6] We analyze the adaptive optics gain over the 5-μrad to 25-μrad seeing range (1064 nm), corresponding to an r_o ($\lambda = 1064$ nm) of 21 cm to 4 cm, respectively.

[5] A. Biswas, S. Lee, G. G. Ortiz, M. Srinivasan, S. Piazzolla, A. Abramovici, D. Losh, C. Lee, and A. Gray, *Pointing, Acquisition and Tracking (PAT) Concept Review for Palomar Receive Terminal (PRT)* (internal document), Jet Propulsion Laboratory, Pasadena, California, August 2004.

[6] D. Mayes, op cit.

To realize gains in optical communications, the adaptive optics system must be designed to correct high spatial frequency wavefront aberrations to allow near-diffraction-limited operation of the receiver. Figure 7 is a simulation of an atmospheric aberrated image as a function of d/r_o or spatial frequency of the wavefront correction. For this simulation, $r_o = 7$ cm. The figure shows that significant improvement in performance can be observed as $d/r_o \Rightarrow 0.5$, where d is the spatial separation of the actuators projected at the telescope pupil.

Figure 8 shows a plot of the angular size of the 80 percent energy enclosed disk as a function of number of actuators across a 1-m aperture for an atmosphere of $r_o = 7$ cm. The 80 percent energy enclosed metric (which comes from the 1-dB signal-loss point) is used throughout this article as the criteria for selecting the required number of actuators and for calculating the corresponding background level. The 1-dB signal loss is the commonly used metric although 80 percent is not necessarily optimum, especially with high backgrounds [2]. The figure shows that, for these conditions, with $N = 100$ actuators ($d/r_0 = 0.14$) across the aperture, the WFE is 25-nm root-mean square (rms), and 80 percent of the energy is enclosed in a 1.5-μrad disk. Under these atmospheric conditions, with $d/r_0 = 0.5$ and $N = 30$, a 50-nm WFE correction can be achieved across the aperture. At this level of wavefront correction, 80 percent of the energy is enclosed in a 4-μrad FOV. From inspection of the encircled energy plot in Fig. 8, we consider an AO system with $d/r_0 = 0.5$ as our design point for the communications system. It is important to note that only the WFE due to atmospheric fitting error is considered in these simulations. Bandwidth calibration errors and measurement noise will add to the residual wavefront error.

Using the sky background noise in Table 2 (the gain realized by adaptive optics increases with background noise level), we calculated the sky background photons received in three slot widths of Table 2 for 5-μrad and 25-μrad seeing. Using an adaptive optics system, the point design of $d/r_0 = 0.5$, i.e., 2.5-cm sub-aperture size (d) corresponding to 25-μrad seeing, will require $N = 40$ actuators per meter of aperture. At this level of correction, the residual WFE is 40 nm, and 80 percent of the energy is enclosed in 3.4 μrad. Under 5-μrad seeing conditions, this corresponds to $d/r_0 = 0.07$, a residual WFE of 30 nm, with 80 percent of the energy enclosed in 2.4 μrad. Table 3 shows that adaptive optics can reduce background flux levels by one order of magnitude in nominal atmospheric conditions, and by two orders under poor seeing conditions.

C. Adaptive Optics Enhancement for the Mars Optical Link

Pulse-position modulation (PPM) is identified as the communications format for the deep-space optical link. In PPM, the data word is constructed by dividing time into M slots, where the number of bits in

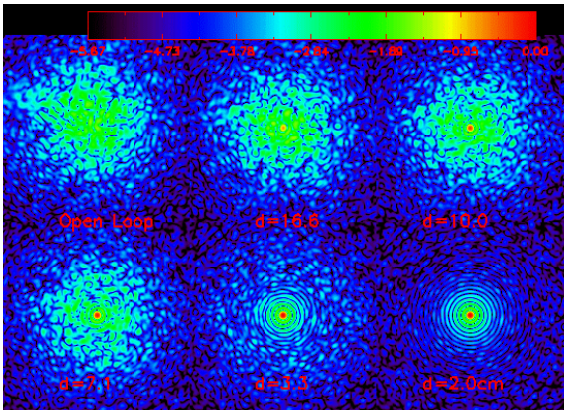

Fig. 7. Improvement in image quality with increasing correction of higher-order spatial frequencies. Only atmospheric fitting error is simulated.

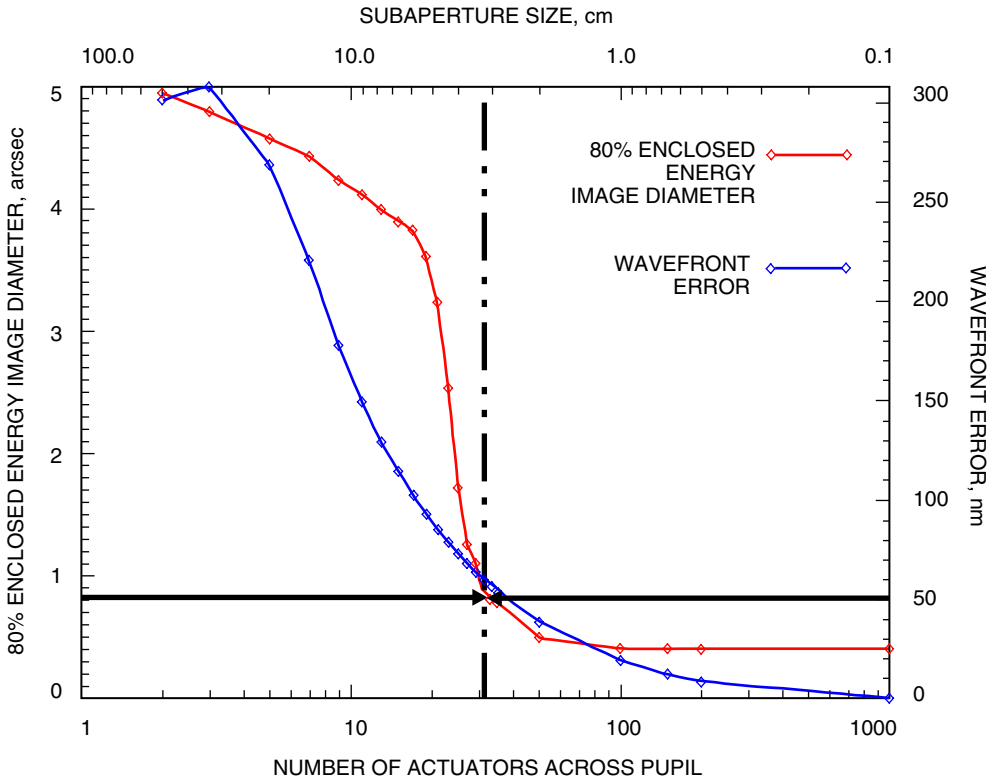

Fig. 8. Plot of the 80% energy enclosed disk versus the number of actuators across the pupil for a 1-m aperture, r_o = 7 cm at 1.065 μm. The vertical line indicates $d/r_0 = 0.5$.

the word is given by $\log_2 M$. Depending on the laser, the slot width for the deep-space link can range from sub-nanoseconds to a few nanoseconds. The bit-error rate (BER) is the metric that quantifies the link performance. This is given in Eq. (4) as a function of the word-error probability (PWE) and PPM order M. The derivation is given in Appendix B.

$$\mathrm{BER} = \frac{1}{2}\frac{M}{M-1}\mathrm{PWE} \tag{4}$$

We have calculated the BER for the noise levels given in Table 3 under the three operational scenarios listed in Table 2. Results are given for the 5-μrad seeing case in Fig. 9, for the 25-μrad seeing case in Fig. 10, and for the nominal Mars background case in Fig. 11. We define the adaptive optics gain as the reduction in signal required to achieve an uncoded BER of 0.01 from the uncorrected case, which was also used in [2].

Figure 9 shows that adaptive optics offers no gain for the best-case scenario of narrow slot width and good seeing (5 μrad). As the slot width is increased to 38 ns, the nominal case, the noise increases, and adaptive optics realizes a 0.8-dB gain even in good seeing conditions. The worst case corresponds to a slot width of 300 ns, resulting in 11 photons per slot in these good seeing conditions. Adaptive optics enables the FOV to be narrowed from 8 μrad to 2.4 μrad for the 80 percent energy enclosed disk, and it realizes 3.2-dB gain.

Table 3. Sky background photons for the best-, nominal-, and worst-case backgrounds taken from Table 2 and scaled for the two FOVs (8 and 38 μrad) for a 5-m telescope with a 0.1-nm filter with and without an AO system. Mars background photons are taken from Fig. 5 and scaled for the two FOVs (8 and 38 μrad) for the nominal case with a 0.1-nm filter with and without an AO system.

	No AO		AO, 2.5-cm sub-aperture cell size	
Seeing, μrad	FOV, 80% enclosed energy, μrad	Background photons/slot	FOV, 80% enclosed energy, μrad	Background photons/slot
Day sky background best case				
5	8	8.31×10^{-4}	2.4	7.48×10^{-5}
25	38	2.08×10^{-2}	3.4	1.66×10^{-4}
Day sky background nominal case				
5	8	1.38×10^{-1}	2.4	1.24×10^{-2}
25	38	3.46	3.4	2.77×10^{-2}
Day sky background worst case				
5	8	11.41	2.4	1.02
25	38	285.31	3.4	2.28
Mars background nominal case				
5	8	5.54×10^{-2}	2.4	0.005
25	38	1.38	3.4	0.011

The results in Fig. 10 show that adaptive optics affords a 1.0-dB benefit for the best case, a 4.0-dB benefit for the nominal case, and a 8.4-dB benefit for the worst case under the poor seeing conditions (25 μrad) that might be observed during the daytime at lower altitude stations or when looking at low elevations.

When the spacecraft is in orbit around an outer planet, the Sun-illuminated planet will be a source of background noise. Figure 11 shows the BER for the communications link from Mars with the planet in the FOV. The results in Fig. 11 show that as much as a 3.0-dB adaptive optics gain can be realized even at night with Mars in the FOV.

As is shown in Figs. 9 through 11, the AO gains are larger at higher BERs and smaller at lower BERs. To illustrate this gain difference, the currently planned Mars mission—the Mars Laser Comm Demonstrator (MLCD)—is used as an example. The equivalent uncoded BER to the required coded BER of 10^{-6} is 0.23. Tables 4 and 5 show the improved AO gains for the daytime and nighttime scenarios along with those for a BER of 0.01. The increased gains range from 0.1 dB (daytime best case with 5-μrad seeing) to 2.7 dB (nighttime nominal case with 25-μrad seeing).

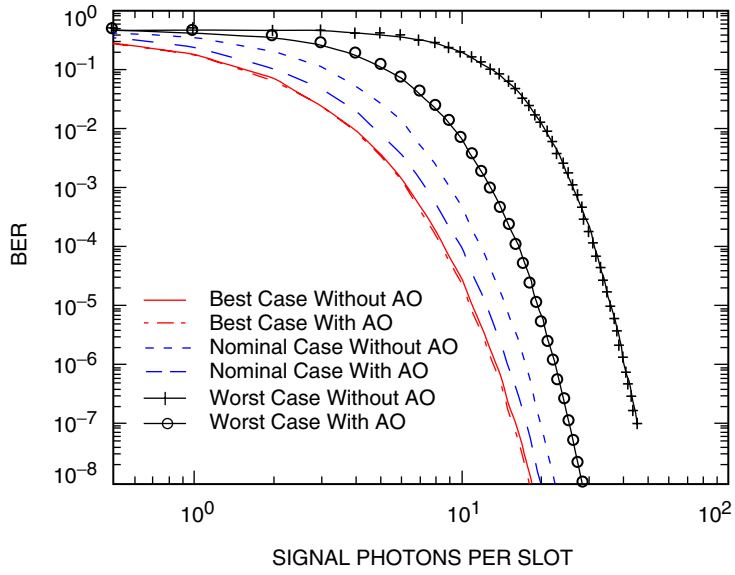

Fig. 9. Daytime BER versus signal photons for 5-μrad seeing. AO gains are 0, 0.8, and 3.2 dB.

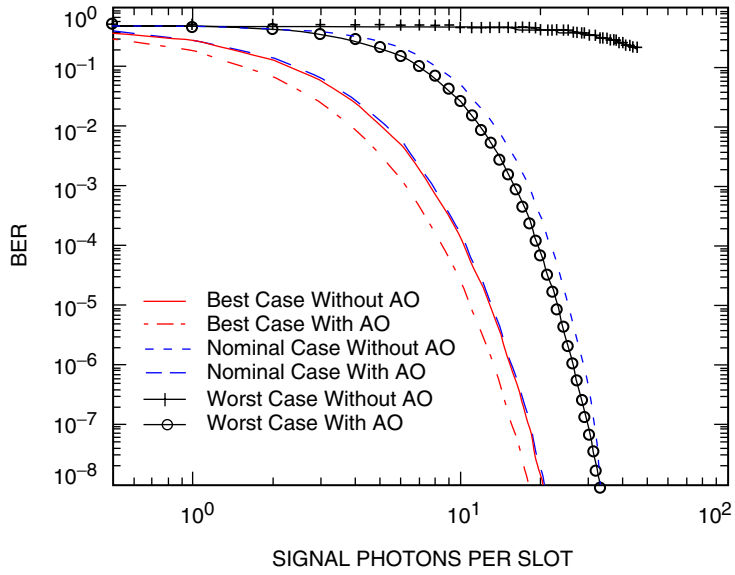

Fig. 10. Daytime BER versus signal photons for 25-μrad seeing. AO gains are 1.0, 4.0, and 8.4 dB.

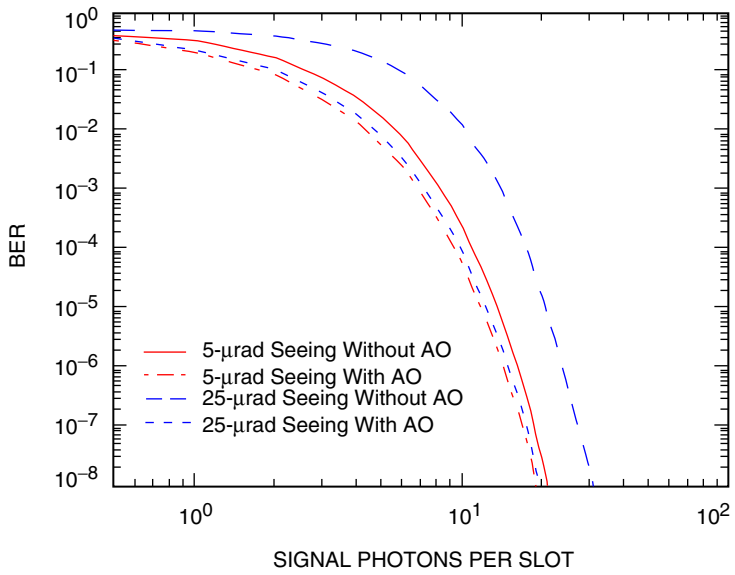

Fig. 11. Nominal Mars case: BER versus signal photons for 5-μrad and 25-μrad seeing. AO gains are 1.0 and 3.0 dB.

Table 4. Daytime AO gains, in dB, for BERs of 0.01 and 0.23.

Case	BER = 0.01		BER = 0.23	
	5-μrad seeing	25-μrad seeing	5-μrad seeing	25-μrad seeing
Best	0.0	1.0	0.1	1.7
Nominal	0.8	4.0	2.4	6.3
Worst	3.2	8.4	4.2	9.5

Table 5. Nighttime AO gains, in dB, of the nominal case for BERs of 0.01 and 0.23.

BER = 0.01		BER = 0.23	
5-μrad seeing	25-μrad seeing	5-μrad seeing	25-μrad seeing
1.0	3.0	2.3	5.7

V. Summary and Conclusion

We have investigated real-world operational scenarios of the deep-space optical communications receiver and assessed the gain afforded by adaptive optics. We have focused on a Mars-to-Earth link and have considered both the day sky and the Sun-illuminated planet at night as sources of background noise. We have considered the effects of atmospheric seeing on the SNR of the link with and without adaptive optics. Our results show that, under nominal background sky conditions, gains of 4 dB can be achieved. In addition, the results show that the background noise from the Sun-illuminated Mars is sufficient to

degrade the link and that adaptive optics can afford a 3-dB enhancement in link performance when Mars is in the FOV of the ground receiver. The AO gains are expected to be larger for the actual deep-space missions since the equivalent uncoded BER is higher than 0.01. Using the uncoded BER of 0.23, derived from the coded BER of 10^{-6} of the MLCD, the AO gains are higher by as much as 2.7 dB.

Currently, laboratory experiments have demonstrated 5-dB gains with an on–off keying (OOK) modulation format, and analysis predicts comparable gains can be achieved with 16-PPM modulation formats and that 4-dB gains can be achieved with 64-PPM modulation [4]. These levels of gains in performance require an advancement of current AO technology. The top-level AO system requirements are $N = 40$ deformable mirror actuators per meter of aperture and operation of daytime AO. JPL currently is exploring developing such high-density actuators for JPL's High Contrast Imaging Testbed [5] program and has $N = 64$ devices. On a 5-m telescope, $N = 200$ or ∼31,000 actuators inscribed in a circle. Although AO systems with this many actuators do not currently exist, many projects, including the Thirty Meter Telescope [6] project, are planning AO systems with ∼10,000 actuators. In a future article, we will address the AO technology and performance issues, such as daytime AO, suitable guide stars, and real-time algorithms, along with system errors such as temporal bandwidth, scintillation, calibration, and measurement.

References

[1] V. Vilnrotter and M. Srinivasan, "Adaptive Detector Arrays for Optical Communications Receivers," *The Telecommunications and Mission Operations Progress Report 42-141, January–March 2000*, Jet Propulsion Laboratory, Pasadena, California, pp. 1–22, May 15, 2000.
http://tmo.jpl.nasa.gov/tmo/progress_report/42-141/141H.pdf

[2] M. Srinivasan, V. Vilnrotter, M. Troy, and K. Wilson, "Adaptive Optics Communications Performance Analysis," *The Interplanetary Network Progress Report*, vol. 42-158, Jet Propulsion Laboratory, Pasadena, California, pp. 1–14, August 15, 2004. http://ipnpr.jpl.nasa.gov/tmo/progress_report/42-158/158B.pdf

[3] J. W. Hardy, *Adaptive Optics for Astronomical Telescopes*, New York: Oxford University Press, 1998.

[4] M. W. Wright, M. Srinivasan, and K. Wilson, "Improved Optical Communications Performance Using Adaptive Optics with an Avalanche Photodiode Detector," *The Interplanetary Network Progress Report*, vol. 161, Jet Propulsion Laboratory, Pasadena, California, pp. 1–13, May 15, 2005.
http://ipnpr/progress_report/42-160/160D.pdf

[5] J. Trauger, "Laboratory Validation of Space Coronagraph Technologies," The Second TPF/Darwin Conference, San Diego, California, July 29, 2004.

[6] R. G. Dekany, B. J. Bauman, D. T. Gavel, M. Troy, B. A. Macintosh, and M. C. Britton, "Initial Concepts for CELT Adaptive Optics," *Proceedings of the SPIE*, vol. 4839, pp. 1165–1174, 2003.

[7] R. M. Gagliardi and S. Karp, *Optical Communications*, New York: John Wiley & Sons, Inc., 1995.

[8] B. Moision and J. Hamkins, "Deep-Space Optical Communications Downlink Budget: Modulation and Coding," *The Interplanetary Network Progress Report 42-154, April–June 2003*, Jet Propulsion Laboratory, Pasadena, California, pp. 1–28, August 15, 2003.
http://ipnpr.jpl.nasa.gov/tmo/progress_report/42-154/154K.pdf

Appendix A

Derivation of the Relationship Between the Required Receiver FOV for a 1-dB Loss and the Seeing Disk

Start with the normalized Gaussian intensity distribution:

$$I(\rho) = \frac{1}{2\pi\sigma^2} e^{-(\rho^2/2\sigma^2)} \tag{A-1}$$

The full width at half maximum (FWHM) of this Gaussian is

$$\begin{aligned} \text{FWHM} &= 2\sigma\sqrt{-2\ln(0.5)} \\ &\approx 2.3548\sigma \end{aligned} \tag{A-2}$$

The 80 percent energy enclosed is determined by integrating Eq. (A-1) so that

$$0.8 = \int_0^{\rho} I(\rho)\rho d\rho \int_0^{2\pi} d\phi$$

$$0.8 = \left(1 - e^{-0.5(\rho_{80\%}/\sigma)^2}\right)$$

The diameter of the circle, s, with 80 percent energy is thus

$$\begin{aligned} s &= 2\rho_{80\%} \\ &= 2\sigma\sqrt{\big(-2\ln(0.2)\big)} \end{aligned} \tag{A-3}$$

From Eqs. (A-2) and (A-3), the relationship between the FWHM and the diameter of the 80 percent enclosed energy is given by

$$\begin{aligned} FOV_{80\%} &= \text{FWHM}\sqrt{\frac{\ln(0.2)}{\ln(0.5)}} \\ &\approx 1.5238\text{FWHM} \end{aligned} \tag{A-4}$$

Appendix B

Derivation of BER Equation for Signal and Background

The probability of word error for a given PPM order M and signal and background levels K_s and K_b [7] is given below in Eq. (B-1). Starting with this equation, we derive the expression for the word-error probability (PWE) equation, Eq. (B-2), and the bit-error rate (BER) equation, Eq. (B-3), for a given PPM order M:

$$\begin{aligned}\mathrm{PWE}(M, K_s, K_b) = 1 &- \frac{\exp\big[-(K_s + MK_b)\big]}{M} \\ &- \sum_{k_1=1}^{\infty} Pos(k_1, K_s + K_b) \left[\sum_{k_2=0}^{k_1-1} Pos(k_2, K_b)\right]^{M-1} \\ &- \sum_{r=1}^{M-1} \frac{(M-1)!}{r!(m-1-r)!(r+1)} \\ &\times \sum_{k=1}^{\infty} Pos(k, K_s + K_b)\big[Pos(k, K_b)\big]^r \left[\sum_{j=0}^{k-1} Pos(j, K_b)\right]^{M-1-r}\end{aligned} \tag{B-1}$$

Equation (B-1) can be simplified to [8]

$$\mathrm{PWE}(M, K_s, K_b) = 1 - \sum_{j=0}^{\infty} \frac{e^{-K_s}}{M} \left(1 + \frac{K_s}{K_b}\right)^j \left(b_{j+1}^M - b_j^M\right) \tag{B-2}$$

where

$$b_j = \sum_{m=0}^{j-1} \frac{K_b^m}{m!} e^{-K_b}$$

The BER is given by

$$\mathrm{BER} = \frac{1}{2} \frac{M}{M-1} \mathrm{PWE} \tag{B-3}$$